

Effect of Gr/Re on Mixed Convection and Combined Mixed Convection-Radiation Heat Transfer Within a Vertical Channel with Variable Wall Temperature

F. Bazdidi-Tehrani* and M. Nezamabadi¹

The present paper investigates, numerically, the effect of the Grashof number to a Reynolds number ratio (Gr/Re), on fluid flow and heat transfer within a vertical channel for two cases: Mixed (natural-forced) convection and combined mixed convection-radiation. The flow in the channel is assumed to be two-dimensional, laminar and steady. The wall temperature is defined as a linear function of the channel height. When dealing with the combined mixed convection-radiation case, radiational properties have been taken into account, both for the walls and the fluid. The fluid has a Prandtl number of 0.71 and it is radiationally assumed as a participating medium. A comparison between the two cases at a constant Gr/Re is reported, so as to investigate the influence of radiation, as one of the heat transfer modes, more clearly. To solve the governing equations (i.e., mass continuity, momentum and energy) the Finite Volume method is employed and the SIMPLE algorithm is adopted to couple the velocity and pressure fields. The radiative transfer equation is solved using the Discrete Ordinates Method, by adopting its S_4 order quadrature scheme. The results for both cases are presented as the profiles of axial velocity across the channel width, axial centerline velocity, bulk temperature and pressure versus channel height.

INTRODUCTION

The problem of heat transfer within vertical channels is one of the interesting topics in the field of heat transfer. This is due to the various applications, among which one may indicate the cooling of electronic equipment, heat exchangers, air conditioning systems and solar collectors.

At first glance, it seems that convection is the governing mode of heat transfer while, if there is a significant difference between the temperature of channel walls or the working fluid and walls, then, radiation is also of noticeable importance. In other words, the

problem comprises a combination of convective and radiative heat transfer. This topic has drawn a great deal of attention from many researchers over the past years.

Mixed convection in vertical ducts has been investigated extensively [1-4] but analyses, including multi-mode heat transfer, are very scarce.

Carpenter et al. [5] have carried out a numerical solution for combined mixed convection-radiation heat transfer within vertical parallel plates, assuming a laminar developing flow. The walls are exposed to an asymmetric wall heat flux and only the effect of wall emissivity is considered.

Gururaja Rao et al. [6] have investigated the influence of radiation from the walls on mixed convection within a vertical channel. Two flush-mounted discrete heat sources have been installed on the walls, having a certain distance from the channel inlet. The walls have a finite thickness and it is assumed that the heat transfer along the height of the wall is dominated by

*. Corresponding Author, Department of Mechanical Engineering, Iran University of Science and Technology, P.O. Box 16844, Tehran, I.R. Iran.

1. Department of Mechanical Engineering, Iran University of Science and Technology, P.O. Box 16844, Tehran, I.R. Iran.

conduction. In this work, the working fluid (air, $Pr = 0.71$) is considered as a radiationally nonparticipating medium.

Slimi and Ben Nasrallah [7] have presented a numerical solution for combined natural convection-radiation within a vertical channel. The channel is filled with a porous medium and the flow is assumed laminar and unsteady.

Recently, a numerical study on the basis of the finite volume method of the interaction between thermal radiation and laminar mixed convection for ascending flows of emitting and absorbing gases (H_2O , CO_2 and H_2O-CO_2 mixtures) in vertical tubes has been presented by Sediki et al. [8]. The wall is considered as isothermal. Also, they have reported that the radiation delays the occurrence of reverse flow for heated gases.

Yang [9,10], employing an implicit finite difference scheme, has investigated the combined mixed convection and radiation in a vertical pipe subjected to a uniform wall heat flux and constant wall temperature.

In all the above-mentioned investigations, it has been assumed that there is either a constant temperature or a constant heat flux as the boundary conditions on the walls. Also, in most of them, only the radiative effects of the walls have been taken into account and the working fluid has been assumed to be a non-participating medium. Heat transfer within vertical channels with a variable wall temperature, which is defined as a function of the channel height, involves particular issues, which are studied numerically in the present research. It should also be noted that in the present study of combined mixed convection-radiation, in addition to the effects of wall radiation, the radiative properties of the working fluid, such as emitting, absorbing and scattering, have been taken into account. In this work, the influence of Gr/Re on the quality of heat transfer has been reported separately, for both mixed convection and combined mixed convection-radiation, so as to accomplish a proper comparison between the two cases.

The effects of radiative parameters, such as Planck number, scattering albedo, optical thickness and wall emissivity, on the fluid flow and heat transfer within the present vertical channel, have been studied by the authors [11].

ANALYSIS

A schematic of the physical model alongside the relevant boundary conditions is shown in Figure 1. The channel is composed of two parallel plates. The fluid has a uniform velocity, v_∞ , and a temperature, T_∞ , at the channel inlet. The flow is assumed to be steady and laminar. The fluid is Newtonian and incompressible, having a Prandtl number of 0.71. It is assumed as gray with all of the radiative properties

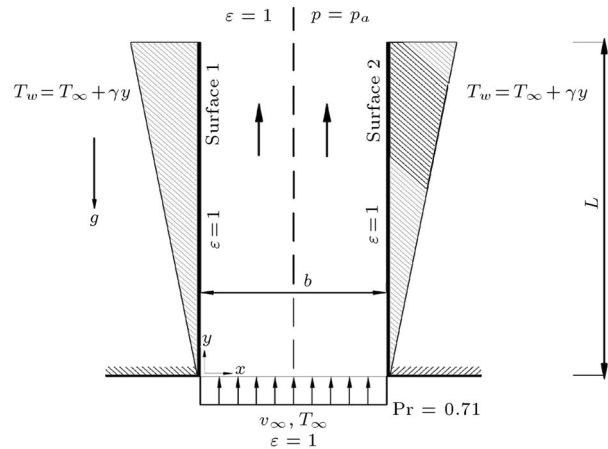


Figure 1. Schematic of the channel geometry and boundary conditions.

(i.e., absorbing, emitting and scattering), and that the scattering is isotropic. At the channel outlet, the pressure is assumed to be fixed and identical to that of the ambient, p_a [7]. The walls temperature is defined as a linear function of the channel height, such that it increases as the channel height increases. Axial conduction along the channel walls is neglected. All thermo physical properties of the fluid, except density, are assumed to be constant. Channel walls are considered as diffuse-gray surfaces and the channel inlet and outlet as black surfaces with $\epsilon = 1$ [5].

Continuity, transverse momentum, axial momentum and energy equations in the non-dimensional form for the combined mixed convection-radiation, under steady and two-dimensional conditions, are as follows:

$$U \frac{\partial U}{\partial X} + V \frac{\partial U}{\partial Y} = 0, \quad (1)$$

$$U \frac{\partial U}{\partial X} + V \frac{\partial U}{\partial Y} = -Re^2 \frac{\partial P}{\partial X} + \frac{\partial^2 U}{\partial X^2} + \frac{1}{Re^2} \frac{\partial^2 U}{\partial Y^2}, \quad (2)$$

$$U \frac{\partial V}{\partial X} + V \frac{\partial V}{\partial Y} = -\frac{\partial P}{\partial Y} + \frac{\partial^2 V}{\partial X^2} + \frac{1}{Re^2} \frac{\partial^2 V}{\partial Y^2} + \frac{Gr}{Re} Y \theta, \quad (3)$$

$$U \frac{\partial \theta}{\partial X} + V \frac{\partial \theta}{\partial Y} + \frac{V \theta}{Y} = \frac{1}{Pr} \left\{ \frac{\partial^2 \theta}{\partial X^2} + \frac{1}{Re^2} \frac{\partial^2 \theta}{\partial Y^2} + \frac{2}{Re^2} \frac{1}{Y} \frac{\partial \theta}{\partial Y} - \frac{\tau^2(1-\omega)}{N} \frac{T_\infty}{T^* Y} \left[\left(1 + \frac{T^*}{T_\infty} Y \theta\right)^4 - \frac{1}{4} \int_0^{4\pi} I d\Omega \right] \right\}, \quad (4)$$

where the dimensionless parameters are defined as

follows:

$$\begin{aligned} X &= \frac{x}{b}, \quad Y = \frac{y}{b\text{Re}}, \quad U = \frac{ub}{v}, \quad V = \frac{v}{v_\infty}, \\ P &= \frac{p - p_a}{\rho v_\infty^2}, \quad \theta = \frac{T - T_\infty}{T_w(y) - T_\infty}, \quad \text{Re} = \frac{v_\infty b}{v}, \\ \text{Gr} &= \frac{g\beta T^* b^3}{v^2}, \quad T^* = \gamma b\text{Re}, \quad I = \frac{i}{\sigma T_\infty^4}, \\ N &= \frac{k(a + \sigma)}{4\sigma T_\infty^3}, \quad \tau = (a + \sigma)b, \quad \omega = \frac{\sigma}{a + \sigma}. \end{aligned} \quad (5)$$

In these equations, the variations of density with temperature are taken into account only for the buoyancy term in Equation 3. Density variation with temperature obeys the Boussinesq approximation [12], as in Equation 6:

$$\rho = \rho_\infty [1 - \beta(T - T_\infty)]. \quad (6)$$

In Equation 4, the ratio of environmental temperature to the modified wall temperature of the walls, (T_∞/T^*) , has appeared, which is assumed to be equal to 0.5.

The last term in this equation is the one relating to the radiative energy source, which is obtained from the solution of the Radiative Transfer Equation (RTE). This equation for the steady state is stated as follows:

$$\begin{aligned} \mu \frac{\partial I}{\partial X} + \xi \frac{1}{\text{Re}} \frac{\partial I}{\partial Y} &= -\tau I + \frac{\tau}{4\pi} \left[4(1 - \omega) \left(\frac{T}{T_\infty} \right)^4 \right. \\ &\left. + \omega \int_0^{4\pi} I d\Omega \right], \end{aligned} \quad (7)$$

where μ and ξ are the direction cosines of the direction, r , with respect to x and y coordinates and I is the radiation intensity. The left hand terms of the above equation indicate the variations of the radiation intensity along r . The three expressions on the left-hand side of this equation indicate changes in intensity, due to absorption and out-scattering, emission and in-scattering, respectively. The presence of a Reynolds number in Equation 7 is as a result of the non-dimensionalization.

The boundary conditions for the present problem are defined as in the following manner:

$$\begin{aligned} \text{at } Y = 0, \quad 0 < X < 1 : \\ U &= 0, \quad V = 1, \quad \theta = 0, \quad \varepsilon = 1, \\ \text{at } 0 < Y < \frac{L}{b\text{Re}}, \quad X = 0 : \\ U &= 0, \quad V = 0, \quad \theta = 1, \quad \varepsilon = 1, \end{aligned}$$

$$\begin{aligned} \text{at } 0 < Y < \frac{L}{b\text{Re}}, \quad X = 1 : \\ U &= 0, \quad V = 0, \quad \theta = 1, \quad \varepsilon = 1, \\ \text{at } Y = \frac{L}{b\text{Re}}, \quad 0 < X < 1 : \\ P &= 0, \quad \varepsilon = 1. \end{aligned} \quad (8)$$

The boundary conditions for radiation intensity emitted by the gray diffuse surfaces in Equation 7 are given by [13]:

$$I(r, \Omega) = \varepsilon I_b(r) + \frac{1 - \varepsilon}{\pi} \int_{n \cdot \Omega' < 0} |n \cdot \Omega| I(r, \Omega') d\Omega', \quad (9)$$

where I_b stands for the radiation intensity of a blackbody in non-dimensional form and at the wall temperature and \mathbf{n} is the unit vector, normal to the surface.

To solve Equations 1 to 4 and 7, which are highly coupled, one needs to yield numerical solution methods. Continuity, momentum and energy equations are solved through the finite volume numerical method. To accomplish this, one needs to divide the entire computational domain into finite control volumes and assume a node for each, whose properties are dominant within the whole control volume. In the vicinity of the walls, non-uniform mesh is used to be able to observe the influences of velocity and temperature boundary layers, in which elements with smaller dimensions are employed near the walls and those with greater dimensions are used in the center of the channel.

The pressure-velocity coupling is achieved through a SIMPLE algorithm. This method is described in detail by Patankar [14]. The system of the resultant simultaneous equations is solved by employing a Tri-Diagonal Matrix Algorithm (TDMA).

The Radiative Transfer Equation (RTE) is solved using the Discrete Ordinates Method (DOM) [13].

Although a variety of methods has been presented to solve RTE in the past decades, DOM has received more attention than any of them. The Monte Carlo and spherical harmonic method ($P - N$) are computationally time consuming. The zonal method is not easily applicable to analyzing a radiatively scattering medium and the Discrete Transfer Radiation Method (DTRM) is only applicable to media lacking scattering properties. On the other hand, most of the methods used to solve RTE do not match with the algorithm adapted in the finite volume method. In the DOM, the solid angle about the location is divided into a finite number of ordinate directions, each with uniform intensity. In this method, the integral term in Equations 4 and 7 is replaced by sums over the ordinate

directions, as represented by Equation 10.

$$\int_0^{4\pi} I d\Omega = \sum_{m'} W_{m'} I_{m'}, \quad (10)$$

where w is a weighting factor and m' stands for an ordinate direction.

After substituting this equivalent in Equations 4 and 7, discretising and integrating over the control volume shown in Figure 2, the following equation is obtained:

$$\begin{aligned} \mu_{m'}(A_e I_{m'e} - A_w I_{m'w}) + \frac{\xi_{m'}}{\text{Re}}(A_n I_{m'n} - A_s I_{m's}) \\ = -\tau I_{m'P} + S, \end{aligned} \quad (11)$$

where S is equal to the two last terms on the right hand of Equation 7 in a discretized form.

What is important in the above equation is the method adopted to relate radiation intensities of control volume surfaces to their nodal values, which is accomplished through using a ‘‘Step Model’’ [15]. According to this method, when the direction cosines of some directions are positive, the following relation is valid.

$$I_{m'n} = I_{m'e} = I_{m'P}, \quad (12)$$

$$I_{m'w} = I_{m'W}, \quad (13)$$

$$I_{m's} = I_{m'S}. \quad (14)$$

If the direction cosines change sign, Equations 12 to 14 will also change.

The directions used in DOM may be chosen arbitrarily, but, in the majority of cases, those which are able to fulfill some of the mentioned conditions in the

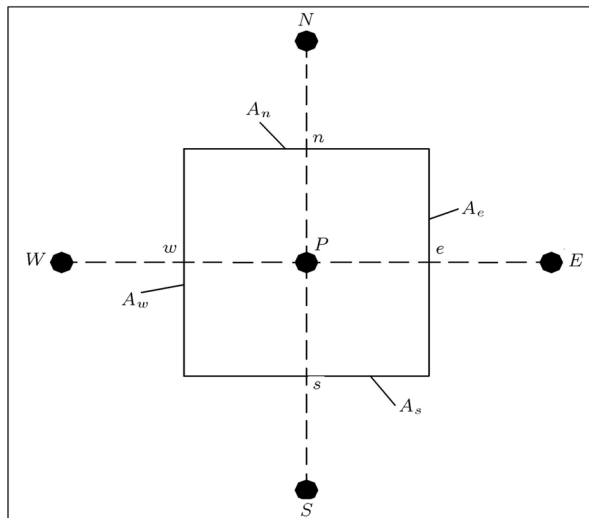


Figure 2. An arbitrary control volume.

Table 1. Ordinates and weights for S_4 quadrature scheme (one quadrant only) [16].

$\mu_{m'}$	$\xi_{m'}$	$\eta_{m'}$	$w_{m'}$
0.295876	0.295876	0.908248	$\pi/3$
0.295876	0.908248	0.295876	$\pi/3$
0.908248	0.295876	0.295876	$\pi/3$

radiative heat transfer problem are recommended. On that basis, the quadrature scheme, S_4 , [16], according to Table 1, has been adopted. This scheme, in addition to not being time-consuming, satisfies both half-range flux and diffuse theory conditions, which are presented in the following relations:

$$\sum_{\mu_{m'} > 0} w_{m'} \mu_{m'} = \pi, \quad (15)$$

$$\sum_{m'} w_{m'} \mu_{m'}^2 = 4\pi/3. \quad (16)$$

There are 24 discrete directions in the S_4 method, but only 12 independent directions and the same number of RTE are considered for each node. The radiation intensity for all the directions of the nodes is computed using a point-by-point method [17]. The coupled equations of continuity, momentum and energy are solved using the following iterative process:

1. An initial guess is made for the velocity, pressure and temperature fields;
2. The RTE is solved, assuming the temperature field specified in step 1;
3. The source term in the energy equation is computed using the result of step 2;
4. Equations 1 to 4 and 7 are solved, simultaneously, so as to compute new velocity and temperature fields;
5. Steps 2 to 4 are repeated until a convergence is achieved for the solution. The criteria employed are as follows:

$$\begin{aligned} \max \left| \frac{\theta_{i+1} - \theta_i}{\theta_i} \right| < 5 \times 10^{-5}, \\ \max \left| \frac{P_{i+1} - P_i}{P_i} \right| < 5 \times 10^{-5}, \end{aligned} \quad (17)$$

where i and $i + 1$ stand for the results of two successive iterations in the solving procedure.

CODE VERIFICATION

To verify the present numerical code, a comparison is made between the present results and those obtained

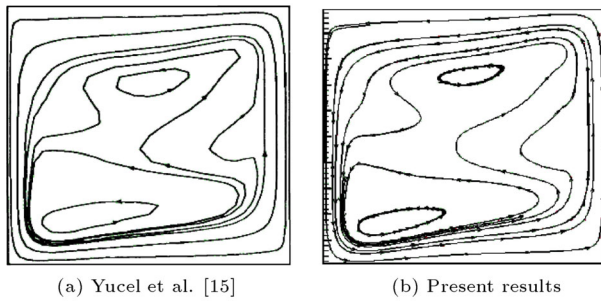


Figure 3. Streamlines in a square enclosure ($Ra = 5 \times 10^6$, $N_e = 0.004$, $\tau_e = 0.2$, $\omega = 0$).

from the reported papers in the literature. The benchmark problem considered here is the numerical solution of combined natural convection-radiation within a 2-D square enclosure [15]. The enclosure is filled with a fluid with the Prandtl number of 0.71 and all of its radiative properties are taken into account. The vertical walls of this enclosure are insulated and the horizontal plates have temperatures T_h and T_c ($T_c/T_h = 0.5$). Figure 3 shows a comparison between the streamlines obtained from the present analysis and those reported by [15]. It can be seen that there is a remarkable agreement between them and, hence, the validity of the present code is verified.

In this analysis, $Ra = g\beta(T_h - T_c)L_e^3/\alpha\nu$, $N_e = k(a + \sigma)/4\bar{\sigma}T_0^3$ and $\tau_e = (a + \sigma)L_e$ where T_0 is the average temperature between T_c and T_h .

GRID SIZE INDEPENDENCY

In order to determine the grid size effect, four different grid sizes have been examined through two different stages as presented in Table 2. In the first stage, the number of control volumes is fixed across the channel width and, in the second stage, the number of control volumes is fixed along the channel height. In each case, V_{\max} and $\theta_{m,\max}$ have been assumed as the comparison values.

These values have been investigated for $Gr/Re = 6000$, $N = 0.1$, $\varepsilon = 1$, $\tau = 1$ and $\omega = 0.5$. In the first stage, by varying the number of the control volumes

Table 2. Grid size independency test ($Gr/Re = 6000$, $N = 0.1$, $\varepsilon = 1$, $\tau = 1$, $\omega = 0.5$).

Stage	$(n_x \times n_y)$	V_{\max}	% Change	$\theta_{m,\max}$	% Change
1	23×72	1.2711	—	0.9685	—
	23×152	1.2739	0.22%	0.9691	0.05%
	23×302	1.2736	0.02%	0.9693	0.03%
2	23×152	1.2739	—	0.9691	—
	43×152	1.2610	1.02%	0.9712	0.23%

from 23×152 to 23×302 , only a deviation of 0.02% in V_{\max} and 0.03% in $\theta_{m,\max}$ is noted. In the second stage, varying the number of control volumes from 23×152 to 43×152 leads to a deviation of 1.02% in V_{\max} , while the difference in $\theta_{m,\max}$ between these grid sizes is 0.23%. Hence, selecting the 23×152 grid size throughout the present work is suitable from both precision and calculation time points of view.

RESULTS AND DISCUSSION

The present numerical solution has been carried out for a fluid with $Pr = 0.71$ and $Re = 50, 500$ and 1000 . When dealing with the combined mixed convection-radiation modes, all the existing radiational parameters, such as the Planck number, N , scattering albedo, ω , optical thickness, τ , and wall emissivity, ε , have been assumed as constant ($N = 0.1$, $\omega = 0.5$, $\tau = 1$, $\varepsilon = 1$) and their effects have been studied extensively in a separate paper by the authors [11]. Also, the ratio, T_∞/T^* , is assumed as constant and equal to 0.5. The parameter, whose variations have been investigated, is the ratio Gr/Re . To analyze its influence, the variation of axial velocity across the channel width and the profiles of axial centerline velocity and bulk temperature along the channel height are presented.

Since, in the incompressible flow, the magnitude of relative pressure is of importance, the variation of this parameter has been studied. It should be noted that, because no important variation occurs in the pressure across the channel width, it is sufficient to present only its variations with the height of the channel. In this work, the relative pressure, P^* , is adopted, according to the following relation:

$$P^* = P - P_\infty, \quad (18)$$

P_∞ has a certain value for each condition in question and can be calculated taking into account each situation. Also, the bulk temperature is defined by:

$$\theta_m = \int_0^1 V \theta dX, \quad (19)$$

where θ_m is evaluated using Simpson's rule [3] and its value versus Y is plotted.

Effect of Gr/Re on Mixed Convection Only

One of the dimensionless parameters, by which the role of natural, compared with that of forced, convection, may be evaluated, is the ratio Gr/Re [1,2]. The lower this ratio, the more the role of forced convection and the higher this ratio, the more the significance of natural convection. So, it is worth studying the influence of this parameter on fluid flow and heat transfer.

It is assumed that the walls and the fluid possess no radiative properties and heat is transferred only by convection. Figures 4 and 5 represent the variations of axial velocity profiles across the channel width, X , for a wide range of ratio Gr/Re of 2000 to 10000 at $Y = 0.1$ and $Y = 0.5$, respectively.

It is observed that the pattern of velocity variations across the channel width is almost the same for all values of Gr/Re. The fluid has its minimum velocity at the center and, as one moves toward the walls, the velocity reaches its maximum. It, then, decreases near the walls and, finally, reduces to zero on the wall. Generally, the main reason for this is the non-uniform distribution of buoyancy force across the channel. In the vicinity of walls, the buoyancy force is higher than that in the channel center. Thus, the fluid is accelerated and its velocity experiences an increase. A rise in the velocity near the walls is followed by a distinct fall in the center, because of the mass flow in the channel being constant and equal to the inlet one.

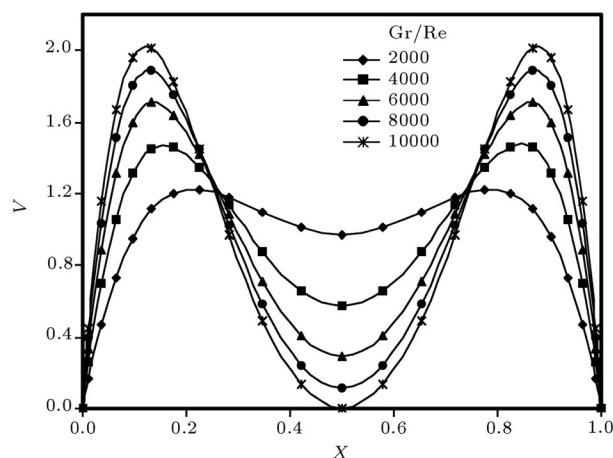


Figure 4. Axial velocity profiles across channel width for various Gr/Re at $Y = 0.1$.

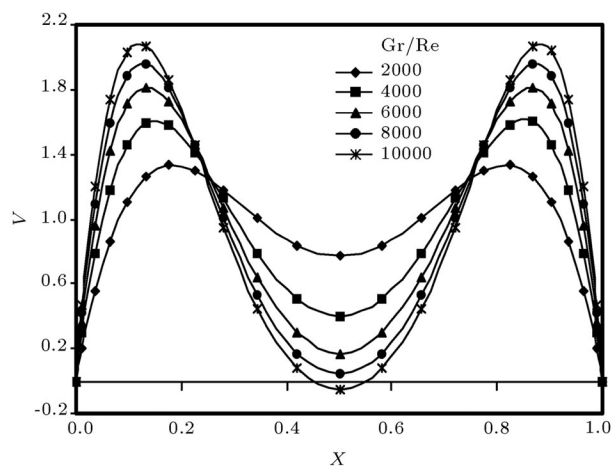


Figure 5. Axial velocity profiles across channel width for various Gr/Re at $Y = 0.5$.

In the present work, because of the linear increase in the temperature of the walls, the non-uniform distribution of buoyancy force across the channel width does not vary at different Y . Thus, no significant variations occur in the velocity profile as one moves up the channel. However, if there existed a constant temperature condition on the walls, then, by moving along the channel, the velocity profile would take up a parabolic shape [3].

Also, it can be seen that the higher the ratio Gr/Re, the more the velocity rise near the wall and the less the velocity in the channel center, such that at Gr/Re = 8000 the flow reversal occurs in the center in the same manner that the mass flow remains constant. The reason for this is that for higher Gr/Re, the buoyancy force has a more non-uniform distribution and, due to the effect of this force on the fluid flow, the most significant variations in the velocity across the channel are observed. The highest and lowest fluid velocity occurs at Gr/Re = 10000.

Figures 6 and 7 demonstrate the axial centerline velocity, V_m , and bulk temperature, θ_m , profiles along the channel for different values of Gr/Re. From Figure 6, it can be seen that at the beginning of the channel, due to the fluid motion being imposed by the inlet conditions (i.e., forced convection), the velocity in the center experiences a rise. In this zone, because of the linear wall temperature distribution (i.e., $T_W = T_\infty + T^*Y$), no significant difference is present between the fluid temperature and T_∞ . Hence, one may deduce that the buoyancy force at the very beginning of the channel is low and, therefore, no effective role is played by natural convection. Then, due to the dominance of natural convection, V_m decreases along the channel. With an increase in the channel length, the wall temperature rises and the working fluid is, as before, affected by these variations. Thus, the velocity

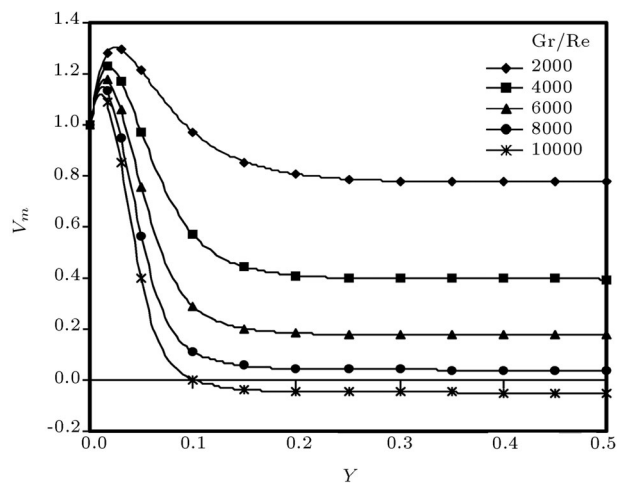


Figure 6. Variations of axial centerline velocity versus channel height for various Gr/Re.

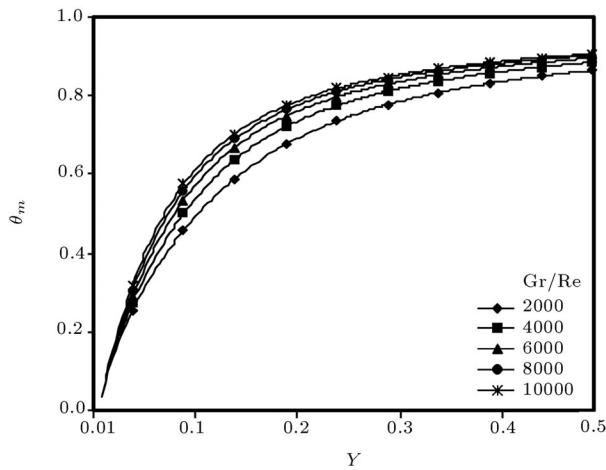


Figure 7. Variations of bulk temperature versus channel height for various Gr/Re .

profiles remain almost unchanged, indicating the fully developed flow condition.

The higher the ratio Gr/Re , the less the length of the channel being influenced by the forced convection. On the other hand, with an increase in Gr/Re , the probability of the flow reversal occurrence rises and the more rapidly hydrodynamic development is attained. The other conclusion inferred from Figure 6 is the fact that at each Gr/Re , the flow develops in a special form. Now, if the boundary condition on the walls were defined as constant temperature one, for all Gr/Re , similar conditions would occur, while the flow would be developing (i.e., a parabolic profile would be gained for the velocity with a maximum value of 1.5 [3]).

Figure 7 indicates that for all Gr/Re , the bulk temperature increases from the entrance region. This figure also shows that for a constant Y , the higher the ratio Gr/Re , the more θ_m will be. Note that with a rise in the ratio Gr/Re , θ_m curve does not vary significantly, such that the above-mentioned profiles for Gr/Re equal to 8000 and 10000 are almost identical and no important differences are distinguished.

Figure 8 depicts the variations of pressure along the channel for different Gr/Re . For all Gr/Re , the pressure at the inlet section initially decreases slightly and, then, increases.

Generally, if there is forced convection within the channel, as one moves upward, a pressure drop will occur due to the shear stress on the wall or, in other words, the friction between the fluid and the wall. Now, if only the natural convection within the channel is under analysis, as the fluid flows up in the channel, the viscous friction tends to decrease the pressure, while the buoyancy force is willing to increase it. So, there is a challenge between these two forces, which leads to the pressure rise along the channel [18].

In the present problem of mixed convection

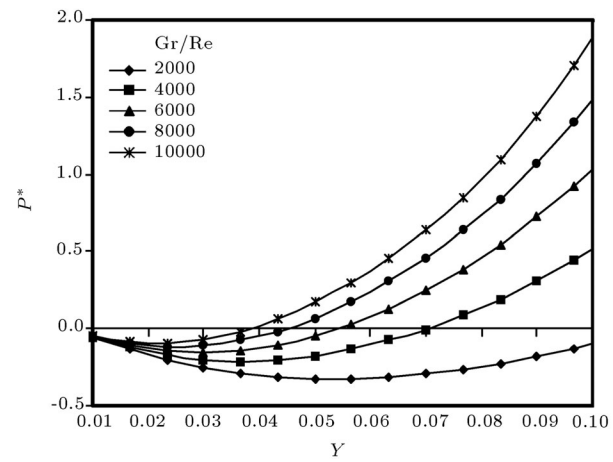


Figure 8. Variations of pressure versus channel height for various Gr/Re .

(forced and natural convection), along with radiation with respect to the value of Gr/Re , there is a pressure fall in the beginning region of the channel and a rise in the pressure magnitude will occur afterwards. It should be noted that the boundary conditions on the wall are chosen so that there is no significant difference between fluid temperature and wall temperature in the beginning region of the channel wall ($T_W = T_\infty + \gamma y$). Hence, in that region, the forced convection acts more strongly than the natural convection. This means a pressure loss, which is confirmed by Figure 8. However, as one moves up along the channel, the influence of the natural convection increases, which results in a pressure rise. As Gr/Re varies, only the amount of variation in pressure and location, where the decreasing behavior is replaced by an increasing one, alters and no difference is observed in the general behavior of the pressure curve.

On the basis of the above-mentioned points, it can be said that the higher the ratio Gr/Re , the less the length of the channel being affected by the forced convection and the more the influence of natural convection in the heat transfer will be.

Effect of Gr/Re on Combined Mixed Convection-Radiation

Figures 9 and 10 illustrate the axial velocity profiles versus the channel width for several values of Gr/Re and at sections $Y = 0.1$ and $Y = 0.5$, respectively. The influence of Gr/Re on the velocity distribution within the channel is closely similar to that of the no radiation case (see Figure 4), in such a way that for $Y = 0.1$, the higher the value of Gr/Re , the more non-uniform distribution for the buoyancy force will come about and, hence, more rises and falls are introduced into the velocity profiles. This fact can particularly be shown for $Gr/Re = 10000$, where the channel center

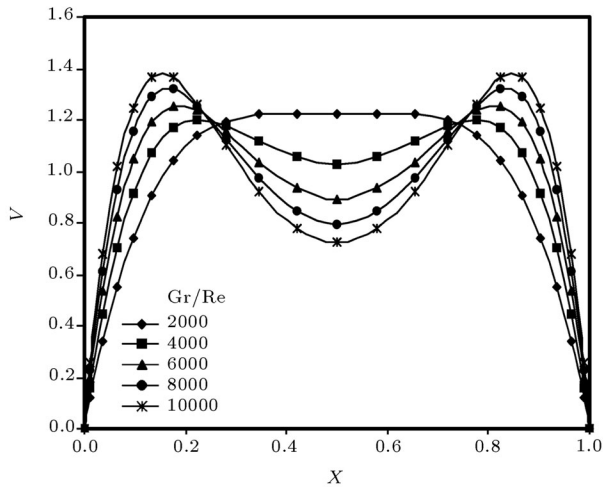


Figure 9. Axial velocity profiles across channel width for various Gr/Re at $Y = 0.1$ (combined mixed convection-radiation, $N = 0.1$, $\varepsilon = 1$, $\omega = 0.5$, $\tau = 1$).

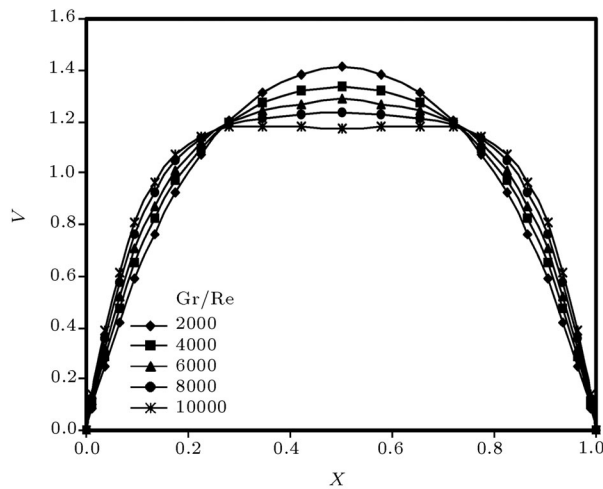


Figure 10. Axial velocity profiles across channel width for various values of Gr/Re at $Y = 0.5$ (combined mixed convection-radiation, $N = 0.1$, $\varepsilon = 1$, $\omega = 0.5$, $\tau = 1$).

demonstrates the least velocity, as compared with the other values of Gr/Re.

With a decrease in Gr/Re, the rate of variation for the velocity profile decreases and there is a tendency to take on a parabolic distribution. The profile for Gr/Re = 2000 confirms this and one expects that for the lower values of Gr/Re, the profile may take up the parabolic shape, right from the very beginning of the channel. From the Gr/Re ratio point of view, the distinct contrast between the radiative and the non-radiative case is in the fact that by taking into account the radiational mode, the velocity profiles are the same for all Gr/Re in the fully developed condition, being a parabolic one. As one goes up along the channel, all the profiles relevant to the various Gr/Re finally lead to a parabolic profile with a maximum velocity of 1.5, in which case, the less the ratio Gr/Re, the more rapidly

the fully developed flow will be attained. This fact is clearly observed in Figure 10.

The main reason for the above-mentioned interactions is the introduction of radiation as an additional mode in the energy transfer phenomenon, which causes a better transfer of heat among molecules of the fluid and, as a result, a more uniform temperature distribution occurs all over the fluid. Consequently, the buoyancy force, which is in close relation with the temperature distributions, also becomes more uniform across the channel and, since the channel center is subject to less shear stress than the walls, the velocity in the center encounters a rise. So, the velocity profile will take on a parabolic shape across the channel.

Figure 11 represents the variations of axial centerline velocity versus height of the channel, taking the radiation mode into account. The lower the ratio Gr/Re, the less the variations of V_m from the beginning up to the end of the channel and, also, the higher the fluid velocity in the channel center will arise.

It can be seen that at Gr/Re = 2000, the hydrodynamic development is reached more rapidly and, in other words, the mixing length is less. The criterion for the hydrodynamic development to occur is to acquire a maximum V_m of 1.5, and almost all the V_m profiles shown for various Gr/Re indicate that this condition will be fulfilled eventually somewhere along the channel.

The profiles of pressure versus height of the channel are illustrated in Figure 12. With an increase in Gr/Re, there will be a slight decrease in the rate of pressure fall at the beginning of the channel, implying the dominance of natural convection. For Gr/Re = 10000, the curve for the pressure variations along the channel has a continuously rising behavior along the channel.

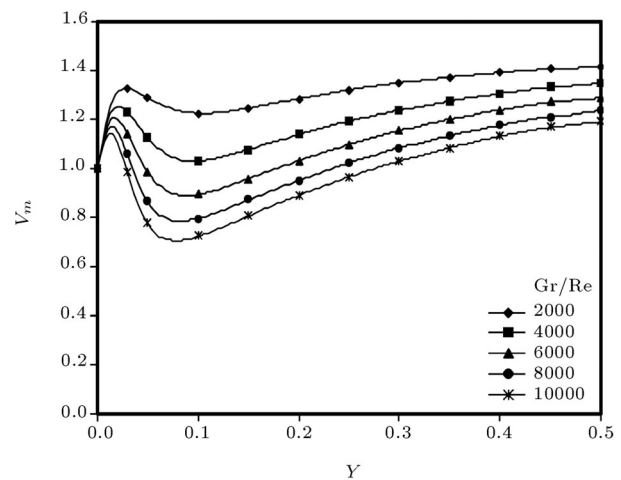


Figure 11. Variations of axial centerline velocity versus channel height for various Gr/Re (combined mixed convection-radiation, $N = 0.1$, $\varepsilon = 1$, $\omega = 0.5$, $\tau = 1$).

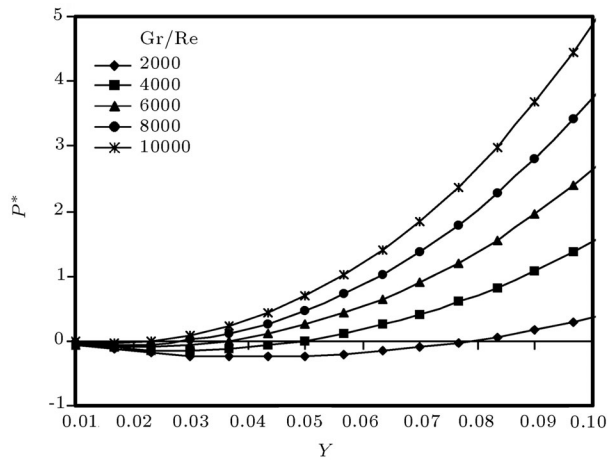


Figure 12. Variations of pressure versus channel height for various Gr/Re (combined mixed convection-radiation $N = 0.1, \varepsilon = 1, \omega = 0.5, \tau = 1$).

Comparison Between Mixed Convection and Combined Mixed Convection-Radiation

To analyze the effect of the presence of radiation mode of heat transfer in the channel, it is appropriate to compare the two cases of mixed convection only and combined mixed convection-radiation. This enables one to clarify the role of radiation thoroughly. In that sense, all the existing parameters common to both cases are assumed as identical, so as to accomplish a valid comparison. The ratio Gr/Re is assumed to be equal to 6000 for both cases.

Figures 13 and 14 show the temperature, θ , and axial velocity, V , profiles across the channel width, X , for the two cases at $Y = 0.1$, respectively.

As depicted in Figure 13, when the influence of radiation is taken into account, the fluid temperature across the whole channel width is higher than that of the non-radiative case. This is also investigated

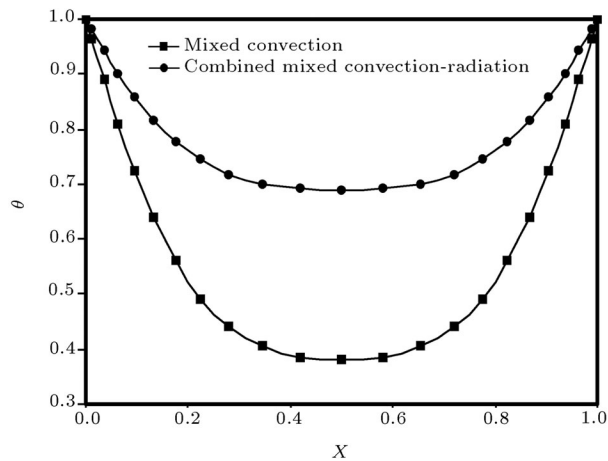


Figure 13. Temperature profiles for mixed convection and combined mixed convection-radiation at $Y = 0.1$ ($Gr/Re = 6000, N = 0.1, \varepsilon = 1, \omega = 0.5, \tau = 1$).

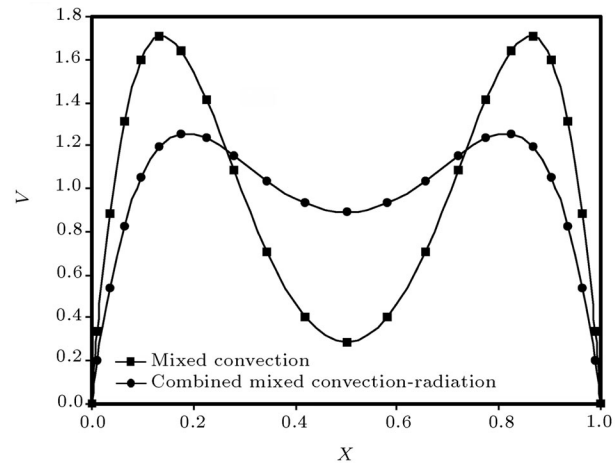


Figure 14. Axial velocity profiles for mixed convection and combined mixed convection-radiation at $Y = 0.1$ ($Gr/Re = 6000, N = 0.1, \varepsilon = 1, \omega = 0.5, \tau = 1$).

to be true at other values of Y . On the other hand, the rate of variation of the temperature for the mixed convection case is higher and, hence, there is a significant difference between the wall and the channel center temperatures.

Figure 14 implies that the rate of variation of the axial velocity for the mixed convection case is higher than that of the radiative case. Because of noticeable variations of temperature near the wall, the buoyancy force accelerates the fluid motion and, since the mass flow is constant and identical to that of the inlet, this velocity increase leads to a decrease of it in the channel center. So, the less the temperature gradient across the channel (equivalent to that of a radiative case), the more uniform the buoyancy force will be obtained and the considerable differences between the extremes of the velocity profiles will diminish.

From Figures 14 and 15, it can be deduced that for the combined mixed convection-radiation case, by

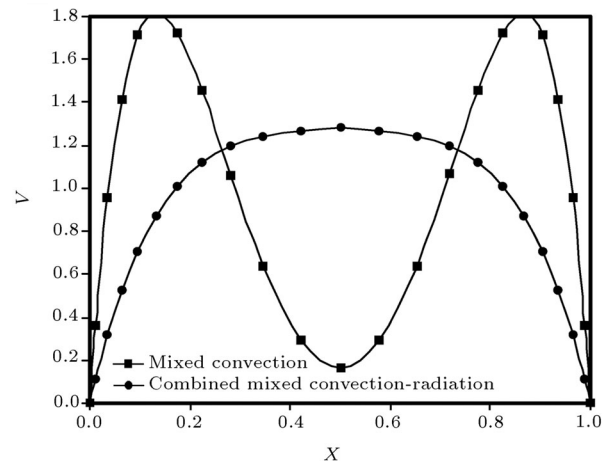


Figure 15. Axial velocity profiles for mixed convection and combined mixed convection-radiation at $Y = 0.5$ ($Gr/Re = 6000, N = 0.1, \varepsilon = 1, \omega = 0.5, \tau = 1$).

moving along the channel (i.e., by increasing Y) the velocity profile tends to become parabolic. But, for the non-radiative case, this does not occur at all and the profile develops in a different manner. The observed differences originate from the fact that by considering the radiative heat flux, as an additional mode of energy transport, there occurs an increase in the thermal diffusion of the fluid. Under this situation, because the heat through the molecules of the fluid is transferred more soundly, the temperature distribution and, as a result the buoyancy force distribution, will be more uniform.

The effect of the presence of radiation is found to be similar to that of a decrease in the Prandtl number. This would be expected, since Pr is defined as the ratio of viscous to thermal diffusion.

Variations of axial centerline velocity and bulk temperature versus the channel height, Y , are depicted in Figures 16 and 17, respectively. Figure 16 shows that for the combined mixed convection-radiation case, the velocity in the channel center is always more than that of the mixed convection case. For the mixed convection case, V_m decreases remarkably and it remains almost constant from the immediate beginning of the channel.

Figure 17 shows that the presence of radiation causes an increase in the bulk temperature, θ_m , throughout the channel, as compared with the non-radiative case.

Figure 18 demonstrates the variations of pressure along the channel height for both cases. The comparison shows that for the combined mixed convection-radiation case, the P^* profile has a falling rate in a shorter length of the channel, which, in turn, indicates that a smaller part of the channel height is under the influence of forced convection. In fact, by analyzing

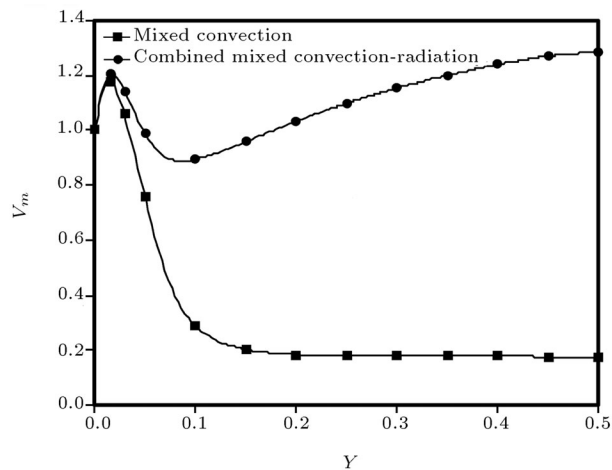


Figure 16. Variations of axial centerline velocity versus channel height for mixed convection and combined mixed convection-radiation ($Gr/Re = 6000$, $N = 0.1$, $\varepsilon = 1$, $\omega = 0.5$, $\tau = 1$).

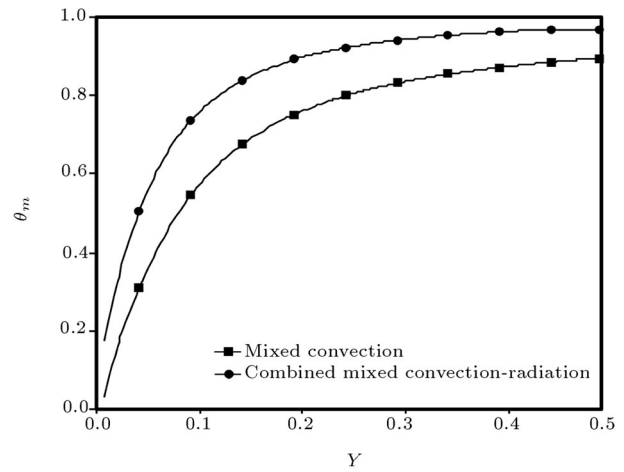


Figure 17. Variations of bulk temperature versus channel height for mixed convection and combined mixed convection-radiation ($Gr/Re = 6000$, $N = 0.1$, $\varepsilon = 1$, $\omega = 0.5$, $\tau = 1$).

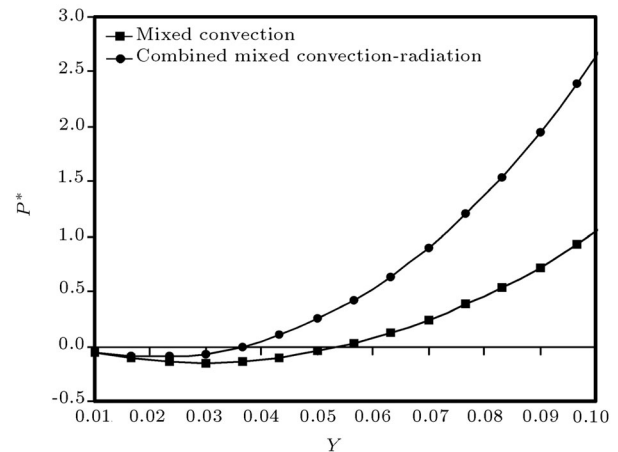


Figure 18. Variations of pressure versus channel height for mixed convection and combined mixed convection-radiation ($Gr/Re = 6000$, $N = 0.1$, $\varepsilon = 1$, $\omega = 0.5$, $\tau = 1$).

the P^* profile, one can conclude that in the combined mixed convection-radiation case, the role of natural convection is more important.

CONCLUSIONS

The present work has been involved with the numerical solution, using the finite volume method, of the mixed convection and the combined mixed convection-radiation heat transfer cases in a vertical channel, in which the effects of radiation for both the walls and working fluid are taken into account. The temperature of the channel walls is variable and is assumed as a linear function of the channel height.

The following points may be concluded:

1. In the mixed convection case, the higher the ratio of Gr/Re , the more the velocity rise near the walls

and the less the velocity in the channel center will be. At $Gr/Re = 10000$, the flow reversal occurs;

2. In the mixed convection case, as one moves along the channel, the velocity profiles remain unchanged, indicating a fully developed condition. In this situation, at each Gr/Re , the flow develops in a special form. In the radiative case, this profile will take on a parabolic shape under the fully developed condition;
3. In the combined mixed convection-radiation case, the lower the ratio of Gr/Re , the less the variations of axial centerline velocity from the beginning up to the end of the channel will be and the more rapidly the fully developed flow will be attained. Also, this velocity is always more than that of the mixed convection case;
4. When the radiation influence is taken into account, the thermal diffusion of the fluid increases. Thus, the temperature distribution and, as a result, the buoyancy force distribution, will be more uniform;
5. In both the combined mixed convection-radiation and the mixed convection cases, as Gr/Re increases, the amount of the pressure fall at the inlet section decreases and, then, the pressure increases at a sharper rate;
6. Generally, the more the value of Gr/Re , the higher the influence of natural convection in the heat transfer within the channel and the less the length of the channel being affected by the forced convection will be.

NOMENCLATURE

a	absorption coefficient, 1/m
b	channel width, m
c	specific heat capacity at constant pressure, J/kg.K
g	gravitational acceleration, m/s ²
Gr	Grashof number
i	intensity, W/m ² .sr
I	non-dimensional intensity
I_b	non-dimensional black body intensity
k	thermal conductivity, W/m.K
L	channel height, m
L_e	height and width of enclosure in the benchmark problem, m
N	Planck number
N_e	Planck number for the enclosure of benchmark problem
n_x, n_y	number of control volumes in x and y directions

p	pressure, Pa
p_a	ambient pressure, Pa
P	dimensionless pressure
P^*	dimensionless relative pressure
Pr	Prandtl number
Ra	Rayleigh number
Re	Reynolds number
T	temperature, K
T^*	modified wall temperature, K
u	transverse velocity, m/s
v	axial velocity, m/s
U	non-dimensional transverse velocity
V	non-dimensional axial velocity
V_m	non-dimensional axial centerline velocity
w	weighting factor
x, y	coordinates in Cartesian system, m
X, Y	dimensionless coordinates in Cartesian system

Greek Symbols

α	thermal diffusivity, m ² /s
β	thermal expansion coefficient, 1/K
ε	wall emissivity
γ	slope of the linearly variable wall temperature, K/m
μ, ξ, η	direction cosines
ν	kinematic viscosity, m ² /s
θ	dimensionless temperature
θ_m	dimensionless bulk temperature
ρ	density, kg/m ³
σ	scattering coefficient, 1/m
$\bar{\sigma}$	Stefan-Boltzmann constant, 5.6697×10^{-8} W/m ² .K ⁴
τ	optical thickness of the medium
τ_e	optical thickness for the enclosure of benchmark problem
ω	scattering albedo
Ω	solid angle, sr

Subscript

m'	ordinate direction
∞	inlet value

REFERENCES

1. Aung, W. and Worku, G. "Developing flow and flow reversal in a vertical channel with asymmetric wall temperatures", *ASME Journal of Heat Transfer*, **108**, pp 299-304 (1986).

2. Aung, W. and Worku, G. "Theory of fully developed, combined convection including flow reversal", *ASME Journal of Heat Transfer*, **108**, pp 485-488 (1986).
3. Ingham, D.B., Keen, D.J. and Heggs, P.J. "Two dimensional combined convection in vertical parallel plate ducts including situations of flow reversal", *Int. J. for Numerical Methods in Engineering*, **26**, pp 1645-1664 (1988).
4. Jackson, J.D., Cotton, M.A. and Axcell, B.P. "Studies of mixed convection in vertical tubes", *Int. J. Heat and Fluid Flow*, **10**(1), pp 2-15 (1989).
5. Carpenter, J.R., Briggs, D.G. and Sernas, V. "Combined radiation and developing laminar free convection between vertical flat plates with asymmetric heating", *ASME J. Heat Transfer*, **98** (1), pp 95-100 (1976).
6. Gururaja Rao, C., Balaji, C. and Venkateshan, S.P. "Effect of surface radiation on conjugate mixed convection in a vertical channel with a discrete heat source in each wall", *Int. J. Heat and Mass Transfer*, **45**, pp 3332-3347 (2002).
7. Slimi, K. and Ben Nasrallah, S. "Study of coupled natural convection and radiation in a porous vertical channel with finite volume method", *European Congress on Computational Methods in Applied Sciences and Engineering ECCOMAS 2000*, Barcelona, Spain (2000).
8. Sediki, E., Soufiani, A. and Sifaoui, M.S. "Combined gas radiation and laminar mixed convection in vertical circular tubes", *Int. J. Heat and Fluid Flow*, **24**, pp 736-746 (2003).
9. Yang, L.K. "Combined mixed convection and radiation in a vertical pipe", *Int. Comm. Heat Mass Transfer*, **18**, pp 419-430 (1991).
10. Yang, L.K. "Forced convection in a vertical pipe with combined buoyancy and radiation effects", *Int. Comm. Heat Mass Transfer*, **19**, pp 249-262 (1992).
11. Bazdidi-Tehrani, F. and Nezamabadi, M. "Numerical analysis of combined mixed convection-radiation in a vertical channel with variable wall temperature", paper submitted to be published at the *Int. J. Thermal Sciences*, Elsevier (2003).
12. Bejan, A., *Convection Heat Transfer*, 2nd Ed., John Wiley and Sons (1995).
13. Siegel, R. and Howell, J.R., *Thermal Radiation Heat Transfer*, 3rd Ed., McGraw-Hill Book Company, New York, USA (1992).
14. Patankar, S.V., *Numerical Heat Transfer and Fluid Flow*, McGraw-Hill, UK (1980).
15. Yucel, A., Acharya, S. and Williams, M.L. "Natural convection and radiation in a square enclosure", *Numerical Heat Transfer*, Part A, **15**, pp 261-274 (1989).
16. Truelove, J.S. "Discrete ordinate solutions of the radiation transport equation", *ASME J. Heat Transfer*, **109**, pp 1048-1051 (1987).
17. Fiveland, W.A. "Discrete ordinate solutions of the radiative transport equation for rectangular enclosures", *ASME J. Heat Transfer*, **106**, pp 699-706 (1984).
18. Oosthuizen, H. and Naylor, D., *Introduction to Convective Heat Transfer Analysis*, McGraw-Hill Book Company, Uk (1999).